Correction of Probe Pressure Artifacts in Freehand 3D Ultrasound*

Graham Treece[1], Richard Prager[1], Andrew Gee[1], and Laurence Berman[2]

[1] Department of Engineering, University of Cambridge, Trumpington Street, Cambridge, UK, CB2 1PZ,
gmt11,rwp,ahg@eng.cam.ac.uk

[2] Department of Radiology, University of Cambridge, Addenbrooke's Hospital, Cambridge, UK, CB2 2QQ,
lb@radiol.cam.ac.uk

Abstract. We present an algorithm which combines non-rigid image-based registration and conventional position sensing to correct probe-pressure-induced registration errors in freehand three-dimensional (3D) ultrasound volumes. The local accuracy of image-based registration enables the accurate freehand acquisition of high resolution (> 15MHz) 3D ultrasound data, opening the way for 3D musculoskeletal examinations. External position sensor readings guarantee the large-scale positional accuracy of the data. The algorithm is shown to increase both the clarity and accuracy of reslices through *in vivo* volumetric data sets.

1 Introduction

Advances in high resolution ultrasound are increasingly enabling detailed examination of musculoskeletal anatomy [2, 8]. However, typical high resolution ultrasound images (B-scans) have a limited field of view: in order to visualise a larger volume, the B-scans must be combined into a composite data set. The most appropriate technique for this is freehand 3D ultrasound, where the probe is moved by hand, and the resulting sequence of B-scans is registered by either intrinsic (image-based) or extrinsic (position sensing) means.

Current position sensing techniques are not able to correctly register high resolution ultrasound data. Limitations in the accuracy of typical position sensors are not the major problem: movement of the anatomy during scanning is a much greater source of error. Even if the patient is still, variation of the pressure of the probe on the skin causes local deformation of the anatomy on a large scale compared to the pixel size (< 0.1mm) in a high resolution B-scan.

Image-based registration, by contrast, has been used successfully to generate extended-field-of-view images [9]. 3D data sets can be constructed by combining image-based registration with speckle de-correlation [6, 7], the latter providing an estimate of the out-of-plane probe movement. These techniques can achieve

* This work was carried out under EPSRC grant GR/N21062. Dynamic Imaging Ltd. provided a modified ultrasound machine to enable digital data acquisition.

W. Niessen and M. Viergever (Eds.): MICCAI 2001, LNCS 2208, pp. 283–290, 2001.

accurate local registration, are fairly robust to noise in the images, and require no user interaction. However, the errors accumulate through a sequence of B-scans.

In this paper, we present a high resolution freehand 3D ultrasound system which uses a combination of non-rigid image-based registration and external position sensing, to provide both local and global accuracy. This robust framework allows us to correct for both pressure-induced and position sensing errors.

To the best of our knowledge, there have been no previous attempts to correct, by non-rigid registration, a sequence of B-scans varying in both time *and* location. Non-rigid registration of two B-scans has been used to track physiological motion [1, 10]. However, such unconstrained registration is only possible if the probe does not move, so all changes can be attributed to tissue movement: even then, substantial regularisation is required. Set in the broader context of image-based registration [3], our work has an important distinguishing feature. While the registration between each pair of images is essentially 2D/2D (the position sensor gives the out-of-plane displacement between consecutive B-scans), we need to make sure that the non-rigid registration corrects only pressure-induced errors, and *not* changes in the image caused by out-of-plane probe movement.

2 Description of the Algorithm

Image-based registration is first performed on a pair of B-scans, the registrations are concatenated over a sequence, then position sensor information is reintroduced to correct any error accumulation.

2.1 Correction of Probe Pressure for a Pair of B-scans

A B-scan is registered to its neighbour by moving it entirely within its own plane, first by a rigid (i.e. x and y) translation, followed by a non-rigid shift in depth (y). Out-of-plane registration is determined solely by the position sensor.

The rigid transformation is calculated from the position of maximum normalised correlation[1] of the pixel intensities within the overlapping region of the B-scans for a range of x and y offsets. Using the whole B-scan, rather than small regions as in block matching [10], de-sensitizes the result to local changes in anatomy. Since the acquisition rate is typically 25Hz, each pair of B-scans is very similar, so the correlation function in x and y approximates the symmetric autocorrelation function, and a simple uphill search for the peak can be used. This symmetry is also useful in interpolating the sub-pixel location of the peak. Given the peak correlation value c_0, and its two neighbours c_{-1} and c_1, the relative offset p from the location of c_0 is given by:

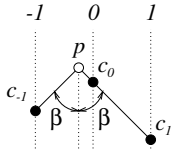

$$p = \begin{cases} \frac{1}{2}\frac{c_1 - c_{-1}}{c_0 - c_1} & \text{if} \quad c_{-1} > c_1 \\ \frac{1}{2}\frac{c_1 - c_{-1}}{c_0 - c_{-1}} & \text{if} \quad c_{-1} < c_1 \\ 0 & \text{if} \quad c_{-1} = c_1 \end{cases} \tag{1}$$

which ensures that the angles β are identical.

[1] There is no observable effect of using the sum of squared difference (SSD) instead.

This gives the relative x and y translation $\{x_c, y_c\}$ of the centre of the new B-scan. However, we already have an estimate of the relative location of the top left corner of the previous B-scan, from the position sensor. The in-plane component of this, described by a translation $\{x_o, y_o\}$ and a rotation α_o, is found by projecting the location of the previous B-scan along the average normal of the two B-scans. The additional in-plane translation $\{x_r, y_r\}$ which should be applied to the new B-scan is therefore:

$$\begin{aligned} x_r &= x_c - 0.5w\,(\cos(\alpha_o) - 1) - 0.5h\sin(\alpha_o) - x_o \\ y_r &= y_c - 0.5h\,(\cos(\alpha_o) - 1) + 0.5w\sin(\alpha_o) - y_o \end{aligned} \tag{2}$$

where w and h are the B-scan's width and height respectively.

This rigid registration is applied before calculating the non-rigid registration, and the previous B-scan is resampled so that it can be directly compared to the subsequent B-scan[2]. Several simplifying assumptions are made in order to calculate the non-rigid component of registration:

- Tissue elasticity is assumed to be uniform across the B-scan, such that probe pressure generates deformation in the y (depth) direction only.
- Tissue elasticity is also assumed to vary slowly with out-of-plane movement. Under this assumption, the shift in anatomy between B-scans will be monotonic with depth, i.e. the entire image is either compressed or expanded.
- It is assumed that both speckle and coherent reflections are deformed in the same way by probe pressure, so both can be used for registration.

The pressure estimate for each B-scan is thus a vector, $P_r(y)$, giving the relative shift in depth at each y. This corrects the most significant effects of probe pressure, while imposing suitable constraints on the registration to prevent it simply following changes in the image due to out-of-plane probe motion.

An initial, noisy estimate of $P_r(y)$, $P_n(y)$ (the dots in Fig. 1) is calculated by correlating each line in the B-scan with nearby lines in the previous (resampled) B-scan, and estimating the peak using (1). $P_n(y)$, which is noisy and not monotonic, can be cleaned up by averaging values of $P_n(y)$ in local neighbourhoods, where the size of the neighbourhood depends on the local variance $v(y)$ of $P_n(y)$: a smaller neighbourhood can be used at depths where $P_n(y)$ is tightly clustered (towards the top of Fig. 1). $v(y)$ is estimated for each y using a small number of neighbouring $P_n(y)$ values. Then, starting with the row y with the lowest variance $v(y)$, the cleaned-up pressure estimate is calculated as follows:

$$P_r(y) = \frac{1}{y_{\text{high}} - y_{\text{low}}} \sum_{i=y_{\text{low}}}^{y_{\text{high}}} P_n(i) \quad \text{where} \quad \sum_{i=y_{\text{low}}}^{y_{\text{high}}} \frac{1}{v(i)} > m, \tag{3}$$

where the range $y_{\text{low}} \ldots y_{\text{high}}$ is symmetrically disposed around y, and the constant m determines the acceptable precision in estimating $P_r(y)$. Values of $P_n(y)$

[2] Rigid alignment in the y direction is only necessary to limit the search space for non-rigid registration, which itself recalculates the y alignment.

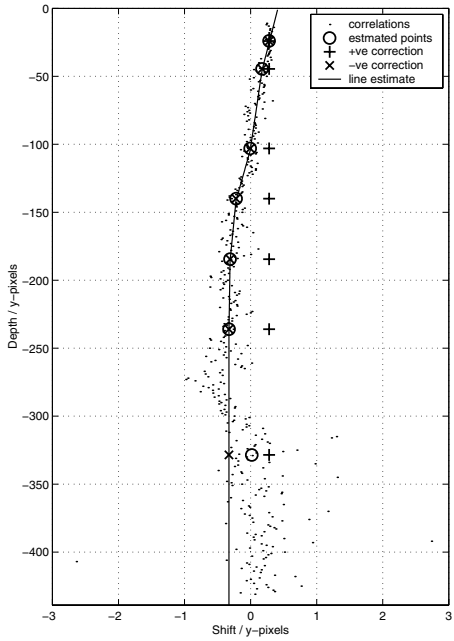

Fig. 1. Estimation of $P_{\mathrm{r}}(y)$.

in the range y_{low} to y_{high} are then discarded, and the process repeated until there are insufficient neighbouring values to satisfy the inequality in (3). The circles in Fig. 1 are seven such estimates of $P_{\mathrm{r}}(y)$: note that there are more in regions where $P_{\mathrm{n}}(y)$ is more tightly clustered.

As these estimates are generated, monotonicity in y is enforced according to the relative depth and value of previous estimates. Both positive and negative adjustments (the crosses in Fig. 1) are investigated: that with the least cost, defined as the sum of the absolute differences between the original and adjusted estimates, is selected. The final $P_{\mathrm{r}}(y)$, shown as a solid line in Fig. 1, is a piecewise linear interpolation of the adjusted pressure estimates. Note that the noisy estimates $P_{\mathrm{n}}(y)$ have been largely ignored at the bottom of the B-scan: this is due to the lack of signal in this region, as apparent in the B-scans in Fig. 2.

2.2 Concatenation of Corrections for a Sequence of B-scans

The final transformation for a B-scan i must take into account all the transformations of the previous B-scans. The location of each B-scan relative to the position sensor reference frame is given by the homogeneous transformation matrix ${}^{\mathrm{p}}\mathbf{T}_{\mathrm{b}i}$ [5]. The B-scan can be moved within its plane by *post*-multiplying ${}^{\mathrm{p}}\mathbf{T}_{\mathrm{b}i}$ with the matrix $\mathbf{T}_{\mathrm{r}}$, calculated from the translation $\mathbf{t}_{\mathrm{r}} = \{x_{\mathrm{r}}, y_{\mathrm{r}}, 0\}^T$:

$$ {}^{\mathrm{r}}\mathbf{T}_{\mathrm{b}i} = {}^{\mathrm{p}}\mathbf{T}_{\mathrm{b}i}\mathbf{T}_{\mathrm{r}}, \quad \text{where} \quad \mathbf{T}_{\mathrm{r}} = \left[\begin{array}{c|c} \mathrm{I} & \mathbf{t}_{\mathrm{r}} \\ \hline 0\ 0\ 0 & 1 \end{array}\right] \tag{4} $$

In order to apply the transformations from previous B-scans without affecting the relative registration, we require the affine *pre*-multiplicative matrix ${}^{\mathrm{r}}\mathbf{T}_{\mathrm{p}i}$ which is equivalent in effect to $\mathbf{T}_{\mathrm{r}}$. The final transformation for B-scan i is:

$$ {}^{\mathrm{r}}\mathbf{T}_{\mathrm{b}i} = {}^{\mathrm{r}}\mathbf{T}_{\mathrm{p}i}{}^{\mathrm{p}}\mathbf{T}_{\mathrm{b}i}, \quad \text{where} \quad {}^{\mathrm{r}}\mathbf{T}_{\mathrm{p}i} = {}^{\mathrm{r}}\mathbf{T}_{\mathrm{p}i-1}{}^{\mathrm{p}}\mathbf{T}_{\mathrm{b}i}\mathbf{T}_{\mathrm{r}}{}^{\mathrm{p}}\mathbf{T}_{\mathrm{b}i}{}^{-1} \tag{5} $$

Unfortunately, the error in ${}^{\mathrm{r}}\mathbf{T}_{\mathrm{b}i}$ will accumulate over a sequence of B-scans. This drift can be corrected by examining the in-plane difference in location $\{x_{\varepsilon i}, y_{\varepsilon i}\}$ between the original (${}^{\mathrm{p}}\mathbf{T}_{\mathrm{b}i}$) and corrected (${}^{\mathrm{r}}\mathbf{T}_{\mathrm{b}i}$) values. In particular, assuming the patient has not moved during the scan, $x_{\varepsilon i}$ should remain within the position sensor tolerance. A simple method of enforcing this constraint is:

- If $x_{\varepsilon i}$ of the last B-scan (i=N) is greater than this tolerance ($\pm$1mm in this case), ${}^{\mathrm{r}}\mathbf{T}_{\mathrm{bN}}$ is reset to ${}^{\mathrm{p}}\mathbf{T}_{\mathrm{bN}}$, and all previous B-scans are adjusted by $\frac{i}{\mathrm{N}} x_{\varepsilon \mathrm{N}}$.
- If the maximum remaining $x_{\varepsilon i}$ is still greater than the tolerance, the process is iterated by resetting this B-scan and adjusting all surrounding scans (up to the closest reset scan) in the same way.

Unlike $x_{\varepsilon i}$, $y_{\varepsilon i}$ must be allowed to be greater than the position sensor tolerance in order to correct for pressure. However, if $y_{\varepsilon i}$ measures the change in y location of the deepest data in the B-scans, one similar correction can be made by removing this error from the final B-scan and adjusting the rest by $\frac{i}{\mathrm{N}} y_{\varepsilon \mathrm{N}}$.

The non-rigid transformation $P_i(y)$ of B-scan i can be calculated simply by adding $P_{\mathrm{r}}(y)$ to the previous non-rigid transformation, allowing for any downward shift y_{offset} in the position of the new B-scan:

$$P_i(y) = P_{\mathrm{r}}(y) + P_{i-1}(y + y_{\mathrm{offset}}) \tag{6}$$

$P_i(y)$ then gives the shift due to pressure relative to the first B-scan. However, $P_i(y)$ may indicate a compression, and we want to *un*-compress the B-scan data. Hence, the B-scan $i = \mathrm{c}$ for which $P_i(y)$ caused the most compression is found, and $P_{\mathrm{c}}(y)$ is subtracted from $P_i(y)$ for all i, using (6). This has the effect of re-registering all the B-scans to c.

Instead of overwriting the original data, the application of $P_i(y)$ and ${}^{\mathrm{r}}\mathbf{T}_{\mathrm{b}i}$ can be toggled in reslice, panoramic, manifold and volume rendering visualisations [4]. This allows a final sanity check on the entire process.

3 Results

B-scans were acquired with a Diasus ultrasound machine[3], using a 10-22MHz linear array probe, on a 4cm depth setting. 8-bit digital log-compressed data was transferred via ethernet at 25Hz to an 800MHz PC running Linux. The probe position was sensed by a Polaris[4] optical tracking system also linked to this PC, and the system calibrated to an accuracy of $\pm$0.35mm RMS. Calibration, acquisition, processing and display of the data was performed by Stradx [4][5]. Pressure corrections were calculated at between 3 and 4 B-scans per second.

Three *in vivo* tests of varying complexity were performed. Figure 2 shows an examination of the common carotid artery and internal jugular vein. Given only a small sideways movement during the scans, the pressure-corrected version of Fig. 2(b) should be similar to the first B-scan in (a). In Fig. 2(c), the positions of the main features are indeed restored, although the shape of the internal jugular is distorted due to the assumption of uniform tissue elasticity: this vessel is at a much lower internal pressure than the carotid. $P_i(y)$ in Fig. 2(d) also shows a change in gradient at the level of the carotid artery, which correctly reflects the more compressible tissue nearer the surface.

[3] Dynamic Imaging Ltd., `http://www.dynamicimaging.co.uk/`
[4] Northern Digital Inc., `http://www.ndigital.com/`
[5] `http://svr-www.eng.cam.ac.uk/~rwp/stradx/`

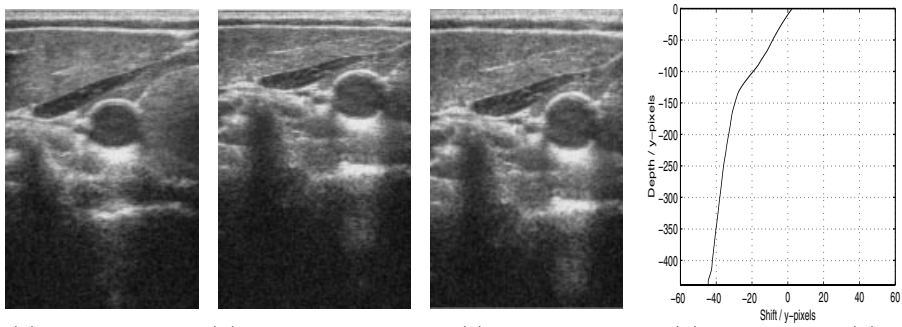

(a) little pressure (b) greater pressure (c) corrected (d) estimated $P_i(y)$

Fig. 2. Correction of probe pressure for repeated B-scans at the same location. (a) and (b) are the first and last B-scans from a sequence of 100 acquired with varying pressure. (c) is the same scan as (b) after correction.

Figure 3 shows a panorama [4] of both lobes of the thyroid, constructed by pasting together data from each B-scan of an approximately planar sequence. In Figs. 3(d) to (g), detail of each panorama is compared with one of the original B-scans. Rigid position correction in (b) and (f) removes the 'jitter' in the image, and non-rigid correction in (c) and (g) removes the local deformation, particularly apparent at the skin surface, and in the shape of the carotid. Note that all of the panoramas are slightly compressed in x relative to the original B-scan: this is a consequence of patient movement, for which we do not attempt to correct.

Figure 4 shows four 3D examinations of the arm, acquired in quick succession with the patient remaining still. Variation of probe pressure causing up to 2mm deformation is clear from the top row of Figure 4(a). This variation is nearly eliminated in the corrected data. Reslices parallel to the skin surface are affected by the poor elevational resolution of the ultrasound beam, as apparent in the lower row of Fig. 4(a). However, the corrected reslices in (b) are much clearer: the path of a small (2mm diameter) vein in the arm is particularly well defined.

Figure 5 shows two examples of pressure-correction applied to lower frequency (3MHz) convex array probes. Physically plausible deformations are calculated in both cases. As would be expected, the top of the bladder is deformed whilst the base stays relatively stationary, despite the sparsity of correlatable features in this data. The top right surface of the liver is also straightened out, even in the presence of pulsatile vascular motion lower down. Other changes in the centre of the scan are due to corrections out of the plane of the reslice.

4 Conclusions

We have presented a novel algorithm, combining image-based and position sensing techniques, to correct the most significant effects of probe pressure in free-

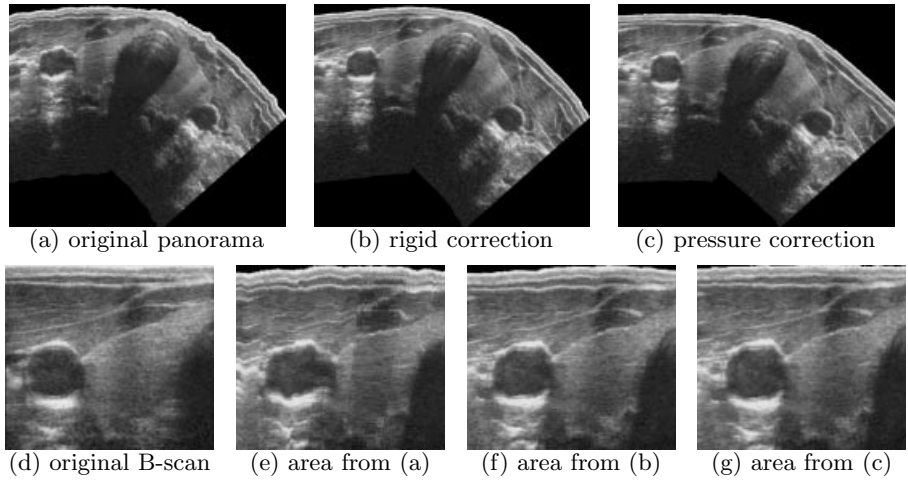

(a) original panorama (b) rigid correction (c) pressure correction

(d) original B-scan (e) area from (a) (f) area from (b) (g) area from (c)

Fig. 3. Correction of probe pressure for a panoramic sequence of B-scans. (a) to (c) show a mosaic of the central data from each B-scan. (e) to (g) show an area from each panorama corresponding to one of the original B-scans in (d).

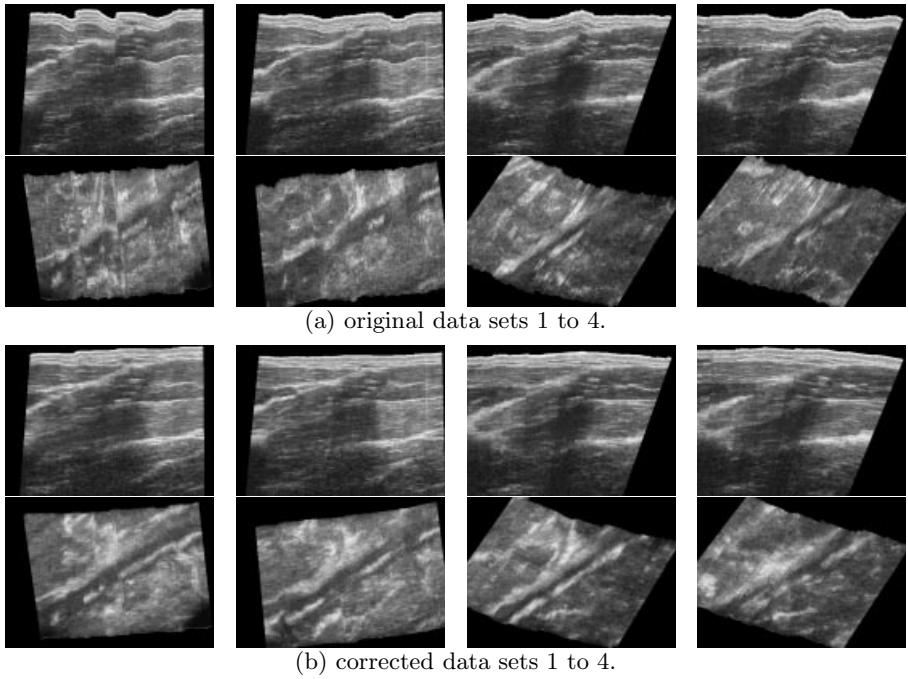

(a) original data sets 1 to 4.

(b) corrected data sets 1 to 4.

Fig. 4. Correction of probe pressure for a freehand 3D volume. (a) shows the same two reslices through four data sets of part of the forearm, the top row perpendicular to the skin surface (and the original B-scans), and the lower row parallel to the skin and about 5mm beneath it. (b) shows the same reslices as in (a) after correction.

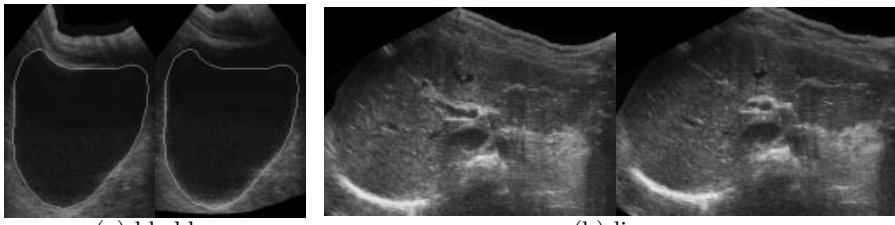

(a) bladder (b) liver

Fig. 5. Correction of probe pressure for lower resolution data. (a) and (b) show original (left) and corrected (right) reslices through data volumes. Both reslices in (a) show the original outline. (b) was acquired in two sequences, each corrected individually.

hand 3D ultrasound data. This increases the clarity of reslices of such data, without compromising global accuracy. There are many possible extensions of this work, including the correct treatment of probe pressure for convex curvilinear probes, and the use of speckle de-correlation for out-of-plane motion correction. A detailed investigation into the limitations and accuracy of the registration algorithm would also be worthwhile.

References

[1] L. N. Bohs, B. H. Friemel, and G. E. Trahey. Experimental velocity profiles and volumetric flow via two-dimensional speckle tracking. *Ultrasound Med Biol*, 21(7):885–898, 1995.

[2] B. D. Fornage, E. N. Atkinson, L. F. Nock, and P. H. Jones. US with extended field of view: phantom-tested accuracy of distance measurements. *Radiol*, 214(2):579–584, 2000.

[3] J. B. A. Maintz and M. A. Viergever. A survey of medical image registration. *Med Image Anal*, 2(1):1–36, Mar. 1998.

[4] R. W. Prager, A. H. Gee, and L. Berman. Stradx: real-time acquisition and visualisation of freehand 3D ultrasound. *Med Image Anal*, 3(2):129–140, 1999.

[5] R. W. Prager, R. N. Rohling, A. H. Gee, and L. Berman. Rapid calibration for 3-D free-hand ultrasound. *Ultrasound Med Biol*, 24(6):855–869, 1998.

[6] W. L. Smith and A. Fenster. Optimum scan spacing for three-dimensional ultrasound by speckle statistics. *Ultrasound Med Biol*, 26(4):551–562, 2000.

[7] T. A. Tuthill, J. F. Krücker, J. B. Fowlkes, and P. L. Carson. Automated three-dimensional US frame positioning computed from elevational speckle decorrelation. *Radiol*, 209(2):575–582, 1998.

[8] S. Wang, R. K. Chhem, E. Cardinal, and K.-H. Cho. Joint sonography. *Radiol Clin N Am*, 37(4):653–668, July 1999.

[9] L. Weng, A. P. Tirumalai, C. M. Lowery, L. F. Nock, D. E. Gustafson, P. L. V. Behren, and J. H. Kim. US extended-field-of-view imaging technology. *Radiol*, 203(3):877–880, 1997.

[10] F. Yeung, S. F. Levinson, and K. J. Parker. Multilevel and motion model-based ultrasonic speckle tracking algorithms. *Ultrasound Med Biol*, 24(3):427–441, 1998.